Supporting Information

©XMU and CCS

Interface-Dependent Nitrite-to-Ammonia Reduction in a Cu/Pd Palladium Membrane Reactor

Bingxin Guo[a], Yaxin Shi[a], Shihe Lin[a], Zhiqin Liang[a, b]*

[a] *School of Physical Science and Engineering, Beijing Jiaotong University, Beijing, 100044 P. R. China*

[b] *Tangshan Research Institute of Beijing Jiaotong University, Xinhua Xi Street 46, Tangshan city, Hebei 063000 P. R. China*

*Corresponding Author: zqliang@bjtu.edu.cn

ACCEPTED

Table of contents

Experimental Procedures.....4

Figure S1. Photograph of the three-compartment palladium membrane reactor (PMR) setup, showing the spatial arrangement of the central membrane working electrode, the isolated hydrogenation chamber, and the two electrolysis chambers equipped with reference and counter electrodes..... 13

Figure S2. Control experiment for the influence of $NaNO_2$ on NH_3 colorimetric detection**.**..13

Figure S3. Hydrogenation-side nitrite reduction performance at 3, 6, and 9 h electrolysis at different applied potentials; (a) apparent Faradaic efficiency referenced to electrolysis-side charge and (b) NH_3 yield rate of the 1.0 mg cm^{-2} Cu/Pd membrane electrode; (c) apparent Faradaic efficiency referenced to electrolysis-side charge and (d) NH_3 yield rate of the 0.5 mg cm^{-2} Cu/Pd membrane electrode.....14

Figure S4. Photograph of the auxiliary-electrode configuration with an additional counter electrode (Pt, Pd, or Cu) introduced into the hydrogenation chamber..... 15

Figure S5. Charging-side chronoamperometric transients during the 30-min pre-electrolysis period for representative auxiliary-electrode/hydrogenation-side control configurations. Labels X–Y denote the membrane electrode (X: Pd or Cu/Pd) and the auxiliary electrode placed in the hydrogenation chamber (Y: Cu, Pd, Pt, or Cu/Pd).....15

Figure S6. Charging-side current-density–time traces recorded during the 9 h hydrogenation-side experiments. (a-d) 1.0 mg cm^{-2} Cu/Pd at -0.4, -0.6, -0.8, and -1.0 V vs. RHE, respectively. (e–g) 0.5 mg cm^{-2} Cu/Pd at -0.4, -0.6, and -0.8 V vs. RHE, respectively. The cathodic current is sustained throughout the reaction period, although the magnitude and degree of temporal variation depend on potential and Cu loading.....16

Figure S7. Control experiments probing hydrogen-supply and material effects. NH_3 yield rates in the two-chamber thermocatalytic control system under acidic (0.1 M H_2SO_4), neutral (0.1 M Na_2SO_4), and alkaline (0.1 M NaOH) electrolytes, and the NO_2^--side electrode was Cu. 16

Figure S8. Enlarged XRD patterns of bare Pd foil and Cu/Pd membrane electrodes with Cu loadings of 0.2, 0.5, and 1.0 mg cm^{-2}. Panels (a–c) show the enlarged diffraction regions corresponding to Pd (111) / Cu (111), Pd (200) / Cu (200), and Pd (220) / Cu (220), respectively.....17

Figure S9. SEM images of Cu/Pd membrane electrodes with different Cu loadings; (a–c) 0.2

ACCEPTED

mg cm^{-2}, recorded at magnifications of 5500×, 2000×, and 1000×, respectively; (d–f) 0.5 mg cm^{-2}, recorded at magnifications of 5500×, 2000×, and 1000×, respectively; (g–i) 1.0 mg cm^{-2}, recorded at magnifications of 5500×, 2000×, and 1000×, respectively.....18

Figure S10. Optical microscopy images (40× magnification) showing the macroscopic surface coverage of Cu/Pd membrane electrodes at Cu loadings of 0.2, 0.5, and 1.0 mg cm^{-2}. 18

Figure S11. Nitrite reduction performance in 0.1 M Na_2SO_4 neutral electrolyte. Heat maps showing the corresponding (a) Faradaic efficiency and (b) NH_3 yield rate across different Cu loadings and applied potentials.....19

Figure S12. Chronoamperometric current-density–time traces for 30-min electrolysis-side nitrite reduction at different Cu loadings and applied potentials. (a–e) 0.1 M NaOH and (f–j) 0.1 M Na_2SO_4, for nominal Cu loadings of 0, 0.2, 0.5, 1.0, and 1.2 mg cm^{-2}, respectively. Each panel includes -0.4, -0.6, -0.8, -1.0, and -1.2 V vs. RHE. These traces show the recorded current-density evolution during the 30-min potentiostatic electrolysis..... 19

Table S1. Average current density (j_{avg}) and total cathodic charge (|Q|) from the 30-min traces in 0.1 M NaOH at -0.8 and -1.2 V vs. RHE (A = 1.77 cm^2; t = 1800 s)..... 20

Figure S13. Cu-only control experiments under the same electrolysis-side nitrite-reduction conditions. (a) NH_3 Faradaic efficiency and (b) NH_3 yield rate of Cu foil in 0.1 M NaOH and 0.1 M Na_2SO_4 over -0.4 to -1.2 V vs. RHE.....20

Figure S14. Schematic illustrations of the paired open-circuit H_2-feeding controls and the corresponding OCP traces: (a, b) H_2 is supplied directly to electrolysis chamber II, bypassing transmembrane hydrogen delivery; (c, d) H_2 is supplied to the hydrogenation chamber and reaches the nitrite-containing interface through Pd-membrane permeation. The pair is used to distinguish the effect of transmembrane hydrogen availability from the effect of open-circuit interfacial operation.....21

Figure S15. Ultraviolet-visible (UV-Vis) absorption spectra and corresponding calibration curves for the quantification of NO_2^- and NH_3.....22

ACCEPTED

Experimental Procedures

Chemicals and Materials.

Sodium nitrite ($NaNO_2$, Adamas, 99.99%), sodium hydroxide (NaOH, Sigma-Aldrich, 99.99% trace metals basis), sodium sulfate (Na_2SO_4, Sigma-Aldrich, ≥99.0%), copper(II) sulfate pentahydrate ($CuSO_4 \cdot 5H_2O$, Sigma-Aldrich, ≥98.0%; 98.0–102.0%, ACS specification), sodium hypochlorite solution (NaClO, Macklin, 10 wt.% in H_2O), ammonium chloride (NH_4Cl, Sigma-Aldrich, ≥99.5%), salicylic acid (Sigma-Aldrich, ≥99.0%), N-(1-naphthyl)ethylenediamine dihydrochloride (Sigma-Aldrich, >98%), sulfanilamide (Alfa Aesar, 98%), sodium nitroprusside dihydrate (Sigma-Aldrich, ≥99%), sodium hydroxide (NaOH, Alfa Aesar, 98%, used for the colorimetric analysis), sodium citrate (Thermo Scientific, 99%), and sodium chloride (NaCl, Thermo Scientific, 99.8%) were used as received without further purification.

The Cu foil used in this work was oxygen-free high-conductivity copper foil (OFHC, 0.008 mm thick, 99.99%, 50 × 50 mm, Thermo Scientific). The Pd foil was palladium foil (0.025 mm thick, 99.9%, 50 × 50 mm, Thermo Scientific). All aqueous solutions were prepared using deionized water. Argon and hydrogen were used as the working gases in the experiments.

Electrode Preparation, Reactor Configuration, and Reaction Procedures

Preparation of Cu/Pd Membrane Electrodes. Commercial Pd foil was cut into 2.5 × 2.5 cm pieces and used as both the substrate electrode and the membrane material. Prior to use, the Pd foil was sequentially rinsed with deionized water and isopropanol, followed by drying under a nitrogen atmosphere.

Cu catalyst layers were deposited onto the Pd foil via potentiostatic electrodeposition. The deposition was carried out in a standard three-electrode configuration using a dimensionally stable anode (DSA) as the counter electrode and an Ag/AgCl reference electrode. The deposition electrolyte consisted of 0.2 M $CuSO_4 \cdot 5H_2O$, 0.5 M H_2SO_4, 0.02 M sodium citrate,

and 0.002 M NaCl. The electrodeposition was performed at a constant potential of 0.25 V vs. RHE under continuous magnetic stirring at 500 rpm. The reported Cu loadings are nominal areal loadings calculated from the electrodeposition charge using Faraday's law and assuming 100% current efficiency for $Cu^{2+} + 2e^- \rightarrow Cu$. The target charge was calculated from $m_{Cu}/A = QM_{Cu}/(nFA)$, with n = 2, M_{Cu} = 63.546 g mol^{-1}, and F = 96485 C mol^{-1}. Nominal Cu loadings of 0.2, 0.5, 1.0, and 1.2 mg cm^{-2} therefore correspond to target charge densities of 0.607, 1.518, 3.037, and 3.644 C cm^{-2}, respectively. Electrodeposition was terminated when the corresponding integrated charge was reached. The Pd foil without Cu deposition was denoted as bare Pd.

Configuration of the Palladium Membrane Reactor and General Electrochemical Conditions. A custom-built, three-compartment palladium membrane reactor (PMR) was employed to construct the spatially separated reaction system. The reactor consisted of electrolysis chamber I, electrolysis chamber II, and a hydrogenation chamber. The prepared Cu/Pd membrane (2.5 × 2.5 cm) was securely fixed in the middle of the reactor, serving simultaneously as the working electrode and the physical separator. The effective geometric area exposed to the electrolyte in the reaction chambers was defined by an O-ring with a diameter of 1.5 cm, corresponding to a geometric active area of approximately 1.77 cm^2. The initial liquid volumes in electrolysis chamber I, electrolysis chamber II, and the hydrogenation chamber were 11.0, 15.0, and 12.0 mL, respectively.

On the electrolysis side, a three-electrode configuration was established with the Pd membrane as the working electrode, a DSA as the counter electrode, and either Ag/AgCl or Hg/HgO as the reference electrode, depending on the electrolyte system. The hydrogenation side was electrically isolated (not connected to any external circuit), ensuring that the hydrogen species at this interface originated exclusively from transmembrane hydrogen permeation.

All potentials were converted to the reversible hydrogen electrode (RHE) scale. All experiments were carried out at room temperature. Electrochemical measurements were

performed using a CHI 760E electrochemical workstation. Before testing the hydrogenation-side reaction, the system was subjected to potentiostatic pre-electrolysis for 30 min to pre-load and condition the Pd membrane before the hydrogenation-side reaction. Representative pre-electrolysis transients are shown in Figure S5, while potential-dependent charging during the subsequent 9-h reactions is shown in Figure S6. Because the charging current is not a direct measurement of hydrogen flux at the opposite membrane surface, this procedure is not taken as proof of a strictly steady transmembrane hydrogen flux. Unless otherwise specified, catalytic data are reported as values obtained under the stated operating conditions.

Nitrite Reduction on the Hydrogenation Side. To investigate nitrite reduction on the hydrogenation side driven solely by transmembrane hydrogen permeation, Cu/Pd membrane electrodes with different Cu loadings were mounted in the palladium membrane reactor. Before each experiment, all compartments were purged with Ar for 15 min to remove dissolved oxygen. During the measurements, 0.05 M H_2SO_4 was introduced into the electrolysis chamber, while 0.1 M $NaNO_2$ was introduced into the hydrogenation chamber. A constant potential was applied on the electrolysis side to drive hydrogen absorption into the Pd membrane. The typical testing potential was -0.6 V vs. RHE, while the effect of potential was also examined from -0.4 to -1.0 V vs. RHE, with the exact range depending on Cu loading (Figure S3). Reactions were typically conducted continuously for 9 h, and liquid samples were collected at different time points to analyze the products formed in the hydrogenation chamber. Unless otherwise specified, the stirring rate was maintained at 500 rpm and the Ar flow rate was fixed at 20 mL min^{-1}. The hydrogenation chamber initially contained 12.0 mL of electrolyte. Samples were collected sequentially at 3, 6, and 9 h. The change in solution volume caused by sampling and the analyte removed in preceding samples were accounted for in the mass-balance calculations described below.

Nitrite Reduction on the Electrolysis Side. To evaluate the promotion effect of the electrolysis-side interface, nitrite was directly introduced into the electrolysis chamber. Cu/Pd

ACCEPTED

membrane electrodes with different Cu loadings were used as the working electrodes. In neutral and alkaline electrolytes, 0.1 M Na_2SO_4 and 0.1 M NaOH were used as the supporting electrolytes, respectively. In both cases, the substrate concentration was fixed at 0.1 M $NaNO_2$. The applied potential range was from -0.4 to -1.2 V vs. RHE. For LSV measurements, the scan rate was set at 10 mV s^{-1}. Potentiostatic electrolysis was performed for 30 min for each test. Liquid products were collected after electrolysis for subsequent colorimetric analysis. Cu-only controls were conducted with the OFHC Cu foil under otherwise identical electrolysis-side nitrite-reduction conditions. Electrolysis-side nitrite reduction occurred in electrolysis chamber II, which initially contained 15.0 mL of electrolyte. Samples used for post-reaction product analysis were collected after completion of the 30-min electrolysis.

Auxiliary Electrode Control Experiments on the Hydrogenation Side. To examine the role of electron participation on the hydrogenation side, an auxiliary electrode was introduced into the hydrogenation chamber and electrically connected to the Pd membrane to create an electron-transfer pathway. Pt, Pd, and Cu were used as the auxiliary electrode materials. All other testing conditions were identical to those used for the hydrogenation-side nitrite reduction experiments. After the reaction, the NH_3 yield in the hydrogenation chamber was determined and compared among different auxiliary electrode materials.

Two-Compartment H_2-Fed Open-Circuit Control Experiments. To evaluate whether a hydrogen-fed open-circuit interface could drive deep nitrite reduction, a two-compartment control cell was used. An H_2-fed electrode/catalyst (Pd, Pd/C, Pt, or Pt/C, as indicated in Figure S7) was placed in one compartment, while a Cu electrode together with nitrite substrate was placed in the other. The two compartments were separated by either a proton-exchange membrane or an anion-exchange membrane to maintain ionic conduction while limiting bulk mixing. Acidic, neutral, and alkaline conditions were established using 0.1 M H_2SO_4, 0.1 M Na_2SO_4, and 0.1 M NaOH, respectively. After 30 min of reaction, samples from both compartments were collected for NH_3 quantification. Because substrate/intermediate crossover and mixed-potential effects cannot be excluded, this

experiment is treated only as a qualitative control. Nitrite crossover was not measured; accordingly, this control is not used to rank intrinsic Cu/Pd activity or assign an intrinsic reaction site.

Open-Circuit H_2-Fed Control Experiments in the Three-Compartment PMR. To evaluate whether a hydrogen-rich interface can sustain deep nitrite reduction without externally imposed polarization, open-circuit controls were performed in the same three-compartment PMR used for the electrochemical measurements. Cu/Pd membranes with different nominal Cu loadings were used, and 0.1 M $NaNO_2$ was always introduced into electrolysis chamber II. Neutral and alkaline conditions were established with 0.1 M Na_2SO_4 and 0.1 M NaOH, respectively.

Two H_2 -feeding configurations were compared specifically to separate transmembrane delivery from open-circuit operation. In the direct-H_2 configuration, H_2 was introduced into electrolysis chamber II, which also contained nitrite, so the Cu/Pd interface contacted H_2 without requiring membrane permeation (Figure S14a). In the permeation configuration, H_2 was introduced into the hydrogenation chamber and reached chamber II only after absorption and transport through Pd (Figure S14c). Both configurations remained at open circuit; the measured OCP is therefore interpreted as a mixed potential established by local anodic and cathodic partial reactions, not as evidence for the absence of interfacial electron transfer.

This paired design provides a practical control to probe the hydrogen-availability-gradient explanation. The permeation configuration can reasonably produce a lower hydrogen chemical potential and/or surface hydrogen coverage at the nitrite-containing interface, whereas the direct-H_2 configuration bypasses the transmembrane transport step while preserving the same open-circuit operating mode. Samples from chambers I and II were collected after 30 min for NH_3 quantification.

Structural and Surface Characterization. X-ray diffraction (XRD) patterns were collected using a Rigaku D/MAX-TTRIII(CBO) X-ray diffractometer (Rigaku Corporation, Japan) to identify the crystalline phases of the Pd substrate and electrodeposited Cu layers. Scanning

ACCEPTED

electron microscopy (SEM) images were acquired using a field-emission scanning electron microscope (JEOL JSM-7001F, Japan), and elemental mapping/energy-dispersive X-ray spectroscopy (EDS) analyses were performed with the attached Oxford INCA X-MAX EDS detector. The SEM magnifications used for the supplementary images are provided in the corresponding figure captions. X-ray photoelectron spectroscopy (XPS) spectra were recorded on a Thermo Fisher Scientific ESCALAB Xi+ spectrometer to analyze surface elemental compositions and chemical states. Survey spectra and high-resolution Cu 2p and Pd 3d spectra were used for the assignments discussed in the main text.

Product measurement and analysis.

Quantification of NH_3. Ammonia was quantified using the indophenol blue method. The salicylic acid/NaOH reagent was prepared by dissolving 4 g NaOH (Alfa Aesar, 98%) in 100 mL deionized water, followed by the addition of 5 g salicylic acid. The sodium citrate solution was prepared by dissolving 5 g sodium citrate in 100 mL deionized water. The 0.05 M NaClO solution was prepared by diluting 3.72 mL of 10 wt% NaClO stock solution to 100 mL with deionized water. The sodium nitroprusside solution was prepared by dissolving 1 g sodium nitroprusside dihydrate in 100 mL deionized water. The salicylic acid/NaOH reagent was stored in a sealed container at 2–8 °C and used within one week. The sodium citrate solution was stored either at room temperature or at 2–8 °C and used within one month. The sodium nitroprusside solution was stored at 2–8 °C and used within one month.

For NH_3 determination, 1 mL of sample was mixed with 0.5 mL salicylic acid/NaOH solution, 0.5 mL sodium citrate solution, 1.0 mL 0.05 M NaClO solution, and 0.1 mL 1 wt% sodium nitroprusside solution. The mixture was allowed to stand at room temperature for 1 h, and the absorbance was measured at 655 nm. The NH_4Cl standards and the calibration curve in Figure S15 were expressed as the mass concentration of nitrogen contained in ammonia (NH_3-N), denoted $C_{NH_3\text{-}N}$. For post-reaction samples, 1.0 mL of electrolyte was typically diluted to 10.0 mL before analysis. If the absorbance exceeded the linear calibration range, an appropriate additional dilution was used and the total dilution factor was applied.

ACCEPTED

For a measured absorbance, the NH_3-N concentration in the diluted analytical solution was obtained from

$$C_{NH3\text{-}N,\ diluted} = \frac{Abs - b}{k},$$

where k and b are the slope and intercept of the NH_3-N calibration curve. The corresponding NH_3 mass concentration was then calculated by applying the molar-mass ratio once:

$$C_{NH3,\ diluted} = C_{NH3\text{-}N,\ diluted} \times \frac{M_{NH3}}{M_N} = C_{NH3\text{-}N,\ diluted} \times \frac{17.03}{14.01}.$$

After correction for the total analytical dilution factor D, the NH_3 concentration in the original electrolyte, total NH_3 mass, and amount of NH_3 were calculated as

$$C_{NH3,\ original} = C_{NH3,\ diluted} \times D,$$

$$m_{NH3} = C_{NH3,\ original} \times V,$$

$$n_{NH3} = \frac{m_{NH3}}{M_{NH3}},$$

where V is the applicable reaction-volume term defined below. The NH_3-N-to-NH_3 conversion was applied only once before calculating both the NH_3 yield rate and Faradaic efficiency.

Quantification of NO_2^-. Nitrite was quantified using the Griess colorimetric method. The Griess reagent was prepared by dissolving 4.0 g sulfanilamide and 0.2 g N-(1-naphthyl)ethylenediamine dihydrochloride in approximately 50 mL deionized water, followed by the slow addition of 10 mL of 85% phosphoric acid. The solution was then diluted to 100 mL with deionized water. The resulting reagent was stored in the dark at 2–8 °C and used within one week.

For NO_2^- determination, the sample was diluted appropriately, followed by the addition of 0.2 mL of Griess reagent. After mixing, the solution was left to stand for 20 min, and the absorbance was measured at 540 nm. The NO_2^- concentration was calculated from a standard calibration curve. In this work, both pre-reaction and post-reaction samples were

ACCEPTED

typically analyzed using a two-step dilution protocol: 1 mL of electrolyte was first diluted to 50 mL, and then 1 mL of the diluted solution was further diluted to 20 mL, corresponding to an overall dilution factor of 1000. Afterward, 0.2 mL of Griess reagent was added, and the absorbance was measured at 540 nm after 20 min.

Analytical Procedure for Reaction Samples. For pre-reaction samples, only NO_2^- analysis was typically performed. Specifically, the electrolyte was diluted stepwise to an overall dilution factor of 1000; 10 mL of the diluted solution was taken followed by the addition of 0.2 mL Griess reagent. Measure the absorbance after letting it stand for 20 minutes. Because no NH_3 was present in the initial electrolyte, NH_3 analysis was generally not performed for these samples.

For post-reaction samples, both NO_2^- and NH_3 were analyzed. The NO_2^- measurement followed the same procedure as that used for the pre-reaction samples. For NH_3 measurement, 1 mL of electrolyte was diluted to 10 mL, followed by the addition of the corresponding colorimetric reagents, and finally measure the absorbance. If the NH_3 concentration was high enough to produce an absorbance value outside the linear range, the sample was further diluted to an appropriate extent before measurement.

Calculation of Performance Metrics.

The NH_3 yield rate was normalized to reaction time and geometric electrode area and is reported in μg h^{-1} cm^{-2}. For electrolysis-side reactions, the Faradaic efficiency for NH_3 formation was calculated from the amount of NH_3 produced and the total charge passed during electrolysis. The total charge was obtained by integrating the recorded current-time response over the 30-min electrolysis period. For hydrogenation-side reactions, the reported value is an apparent Faradaic efficiency referenced to the charge passed on the electrolysis side; because this charge does not directly pass through the floating hydrogenation-side nitrite-reduction interface, this value should be interpreted only as an overall normalization metric for the coupled membrane system. For nitrite-to-ammonia conversion, the electron-transfer number was taken as 6 according to $NO_2^- + 5H_2O + 6e^- \rightarrow NH_3 + 7OH^-$

ACCEPTED

under alkaline notation. Nitrite conversion and NH_3 selectivity were determined from the change in NO_2^- concentration before and after reaction and the amount of NH_3 generated.

For the current-stability analysis associated with Figure S12, the average current density was calculated over the full 1800 s electrolysis as $j_{avg} = (Q \times 10^3)/(A \cdot t)$, using the geometric electrode area A = 1.77 cm^2. The magnitude of the integrated cathodic charge is reported as |Q| in Table S1.

$$\mathrm{Yield}_{NH_3} = \frac{C_{NH_3} V}{tA}$$

$$\mathrm{FE}_{NH_3} = \frac{nFn_{NH_3}}{|Q|} \times 100\%$$

$$NO_2^- \text{ conversion } (\%) = \frac{C_o(NO_2^-) - C_t(NO_2^-)}{C_o(NO_2^-)} \times 100\%$$

$$NH_3 \text{ selectivity } (\%) = \frac{n_{NH_3}}{(C_o(NO_2^-) - C_t(NO_2^-)) \times V} \times 100\%$$

Here, C_{NH_3} is the mass concentration of NH_3 after dilution correction, V is the electrolyte volume, t is the reaction time, A is the geometric electrode area, F is the Faraday constant (96485 C mol^{-1}), n_{NH_3} is the amount of NH_3 produced, Q is the total charge passed during electrolysis, and C_0 (NO_2^-) and C_t (NO_2^-) are the nitrite concentrations before and after reaction, respectively.

For the sequentially sampled 9 h hydrogenation-side experiments, yield, conversion, and selectivity were calculated using a sampling-corrected mass balance rather than a simple concentration × initial-volume calculation.

Sampling correction for the 9 h hydrogenation-side experiments. For each sampling time, cumulative NH_3 formation was calculated by accounting for the NH_3 remaining in the reactor together with NH_3 removed in preceding samples.

The same treatment was applied to the residual nitrite balance, so that nitrite removed during earlier sampling was retained in the substrate mass balance rather than being counted as reacted substrate.

ACCEPTED

Figures and Table

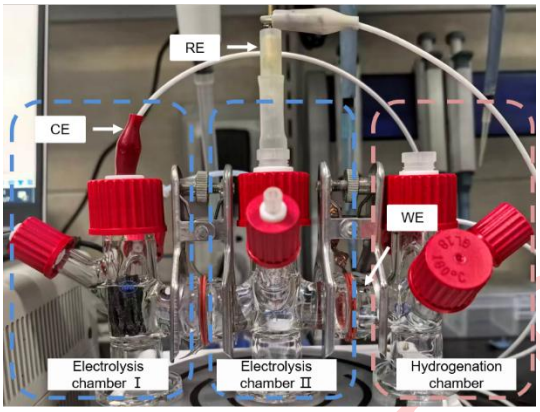


Figure S1. Photograph of the three-compartment palladium membrane reactor (PMR) setup, showing the spatial arrangement of the central membrane working electrode, the isolated hydrogenation chamber, and the two electrolysis chambers equipped with reference and counter electrodes.

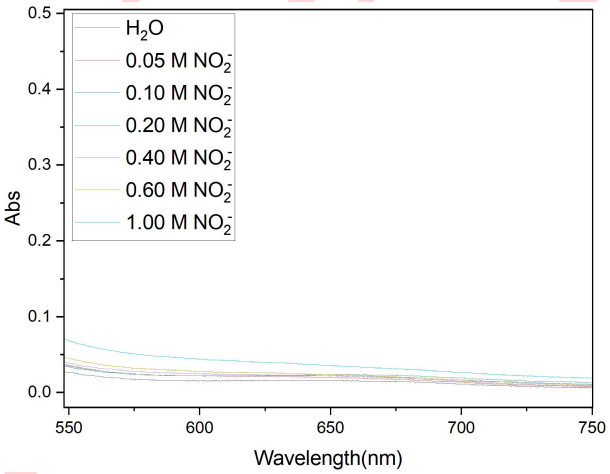


Figure S2. Control experiment for the influence of $NaNO_2$ on NH_3 colorimetric detection**.**

To investigate whether high concentrations of NO_2^- would directly interfere with the indophenol blue ammonia colorimetric determination, we conducted a $NaNO_2$ blank colorimetric control experiment. We prepared solutions of 0.05, 0.10, 0.20, 0.40, 0.60 and 1.00 M $NaNO_2$, and directly added salicylic acid/NaOH, sodium citrate, NaClO and sodium nitroprusside reagents according to the same colorimetric process used in quantitative

ammonia analysis of NH_3 under conditions without electrolysis, without catalyst addition, and without H_2 introduction. After 1 hour of colorimetry, the absorbance was measured.

The results showed that within the range of 0.05-1.00 M $NaNO_2$, the absorbance of the samples was close to the blank value, and no obvious NH_3 color response was observed. This result indicates that under the ammonia detection conditions of this study, $NaNO_2$ itself does not produce a significant false positive NH_3 signal.

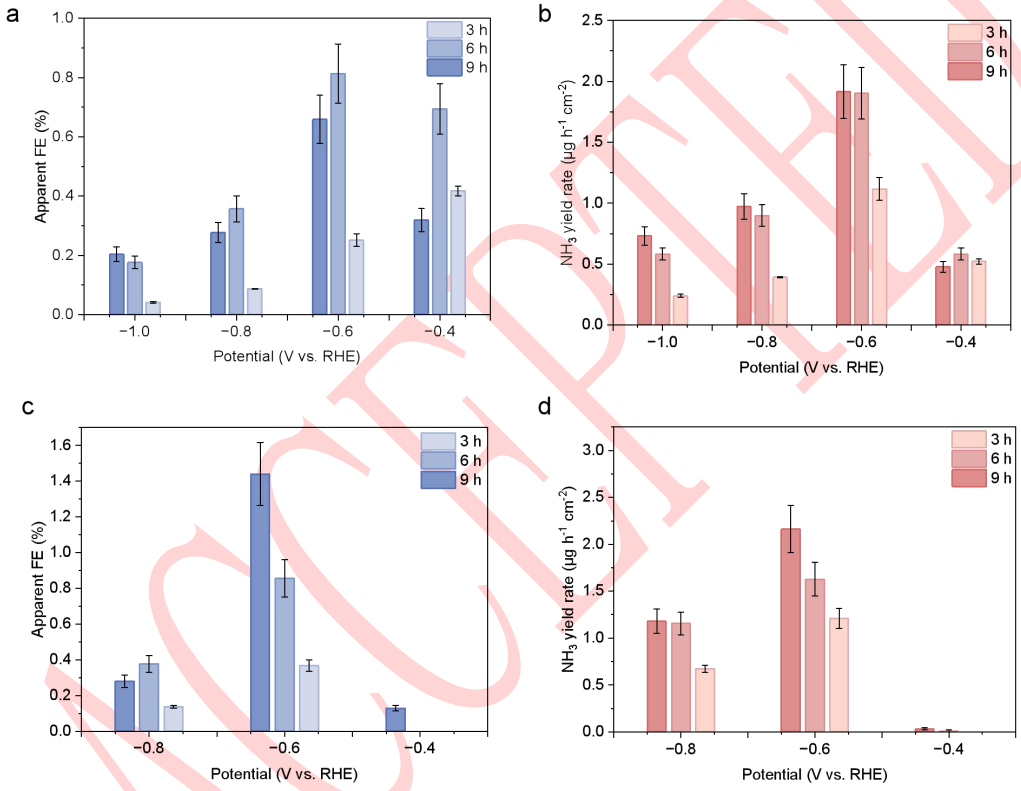


Figure S3. Hydrogenation-side nitrite reduction performance at 3, 6, and 9 h electrolysis at different applied potentials; (a) apparent Faradaic efficiency referenced to electrolysis-side charge and (b) NH_3 yield rate of the 1.0 mg cm^{-2} Cu/Pd membrane electrode; (c) apparent Faradaic efficiency referenced to electrolysis-side charge and (d) NH_3 yield rate of the 0.5 mg cm^{-2} Cu/Pd membrane electrode.

ACCEPTED

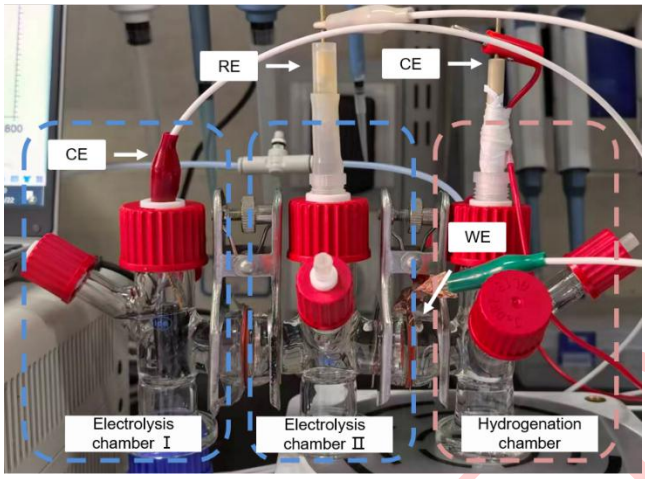


Figure S4. Photograph of the auxiliary-electrode configuration with an additional counter electrode (Pt, Pd, or Cu) introduced into the hydrogenation chamber.

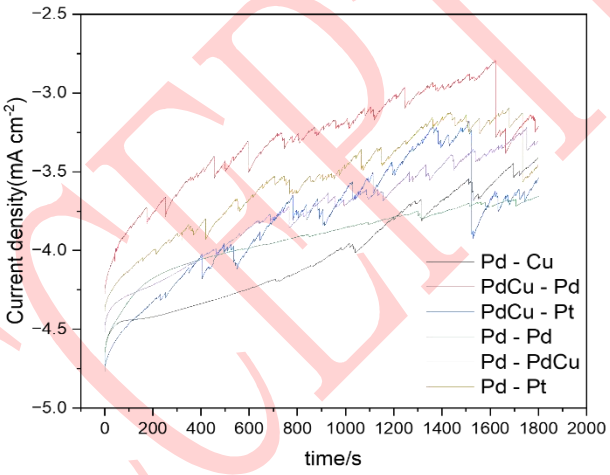


Figure S5. Charging-side chronoamperometric transients during the 30-min pre-electrolysis period for representative auxiliary-electrode/hydrogenation-side control configurations. Labels X–Y denote the membrane electrode (X: Pd or Cu/Pd) and the auxiliary electrode placed in the hydrogenation chamber (Y: Cu, Pd, Pt, or Cu/Pd).

ACCEPTED

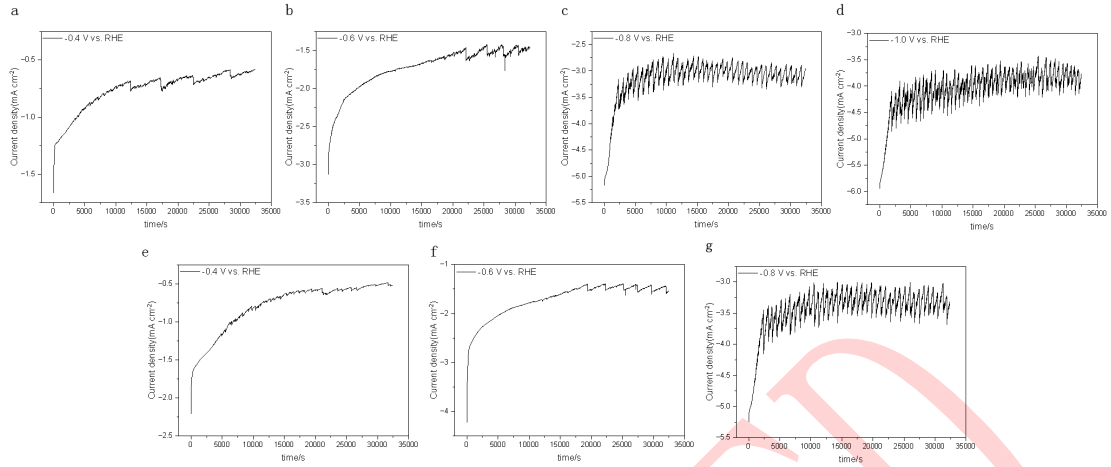


Figure S6. Charging-side current-density–time traces recorded during the 9 h hydrogenation-side experiments. (a-d) 1.0 mg cm^{-2} Cu/Pd at -0.4, -0.6, -0.8, and -1.0 V vs. RHE, respectively. (e–g) 0.5 mg cm^{-2} Cu/Pd at -0.4, -0.6, and -0.8 V vs. RHE, respectively. The cathodic current is sustained throughout the reaction period, although the magnitude and degree of temporal variation depend on potential and Cu loading.

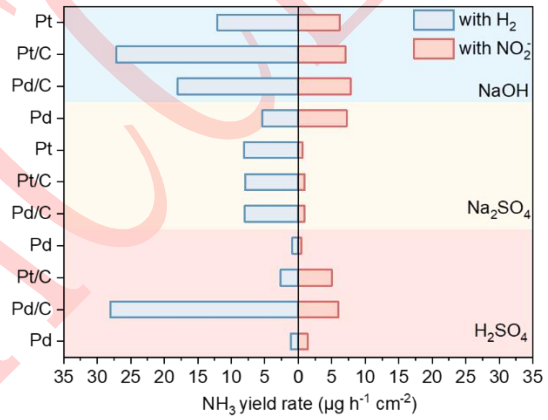


Figure S7. Control experiments probing hydrogen-supply and material effects. NH_3 yield rates in the two-chamber thermocatalytic control system under acidic (0.1 M H_2SO_4), neutral (0.1 M Na_2SO_4), and alkaline (0.1 M NaOH) electrolytes, and the NO_2^--side electrode was Cu.

ACCEPTED

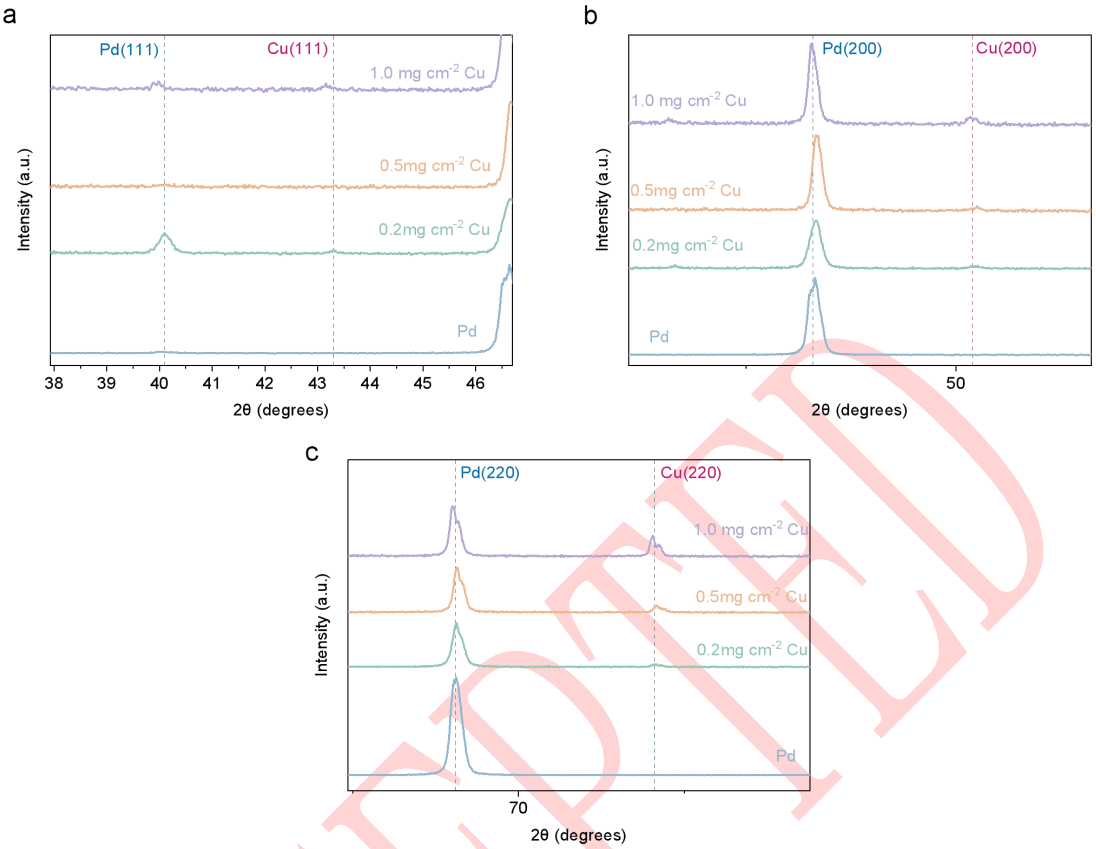


Figure S8. Enlarged XRD patterns of bare Pd foil and Cu/Pd membrane electrodes with Cu loadings of 0.2, 0.5, and 1.0 mg cm^{-2}. Panels (a–c) show the enlarged diffraction regions corresponding to Pd (111) / Cu (111), Pd (200) / Cu (200), and Pd (220) / Cu (220), respectively.

ACCEPTED

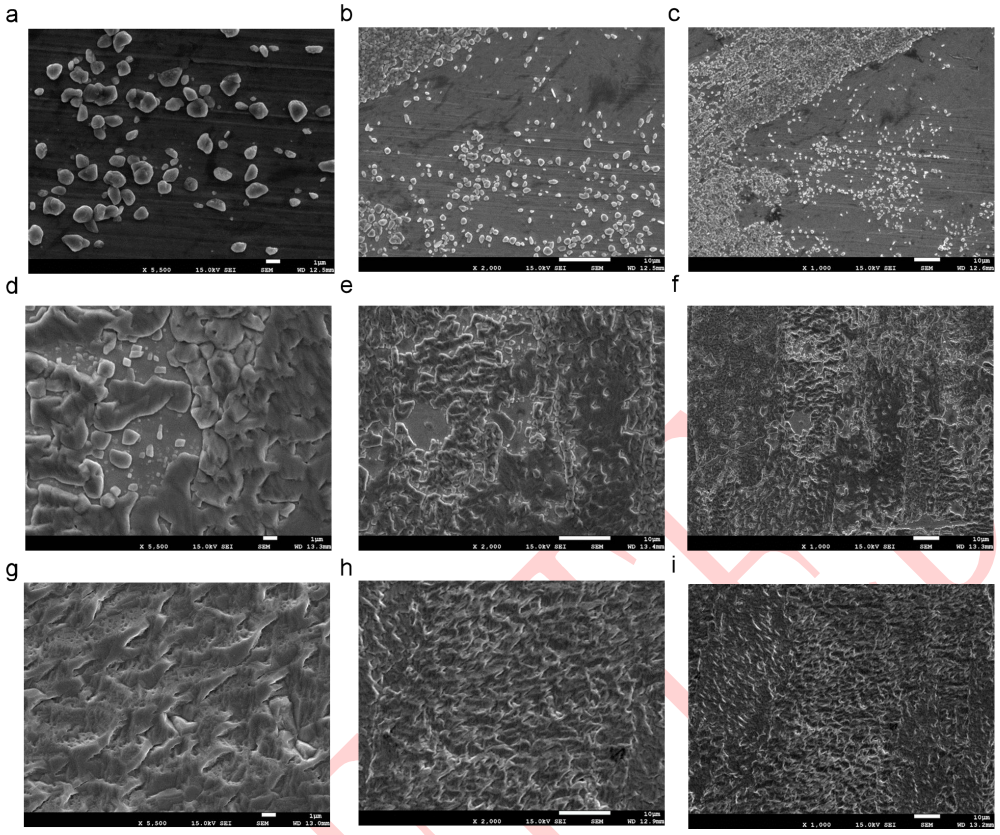


Figure S9. SEM images of Cu/Pd membrane electrodes with different Cu loadings; (a–c) 0.2 mg cm^{-2}, recorded at magnifications of 5500×, 2000×, and 1000×, respectively; (d–f) 0.5 mg cm^{-2}, recorded at magnifications of 5500×, 2000×, and 1000×, respectively; (g–i) 1.0 mg cm^{-2}, recorded at magnifications of 5500×, 2000×, and 1000×, respectively.

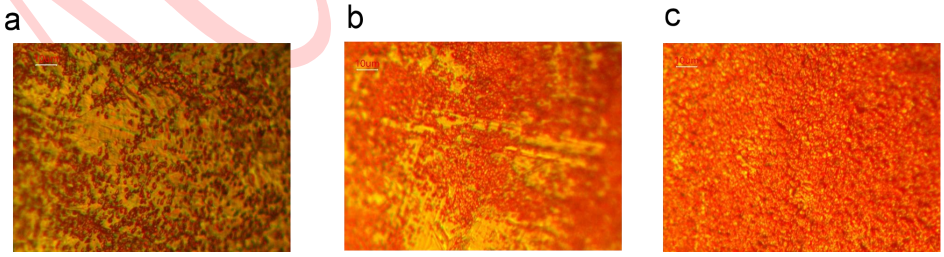


Figure S10. Optical microscopy images (40× magnification) showing the macroscopic surface coverage of Cu/Pd membrane electrodes at Cu loadings of 0.2, 0.5, and 1.0 mg cm^{-2}.

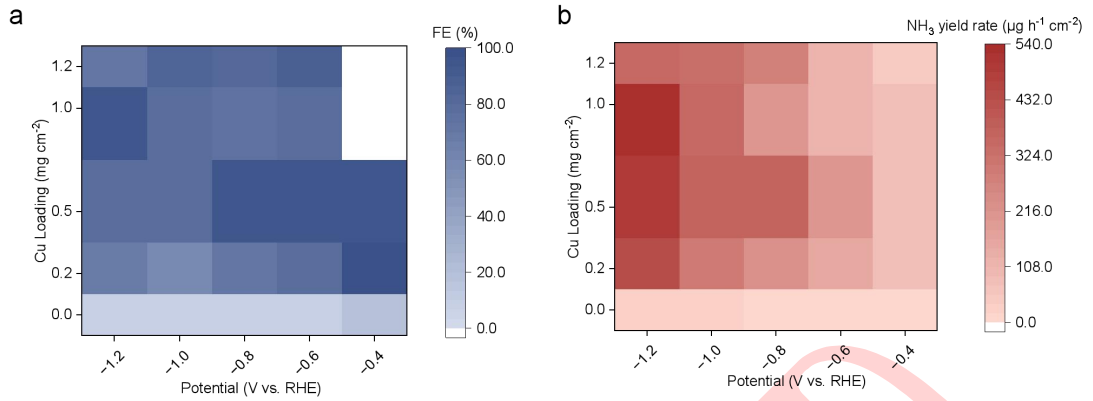


Figure S11. Nitrite reduction performance in 0.1 M Na_2SO_4 neutral electrolyte. Heat maps showing the corresponding (a) Faradaic efficiency and (b) NH_3 yield rate across different Cu loadings and applied potentials.

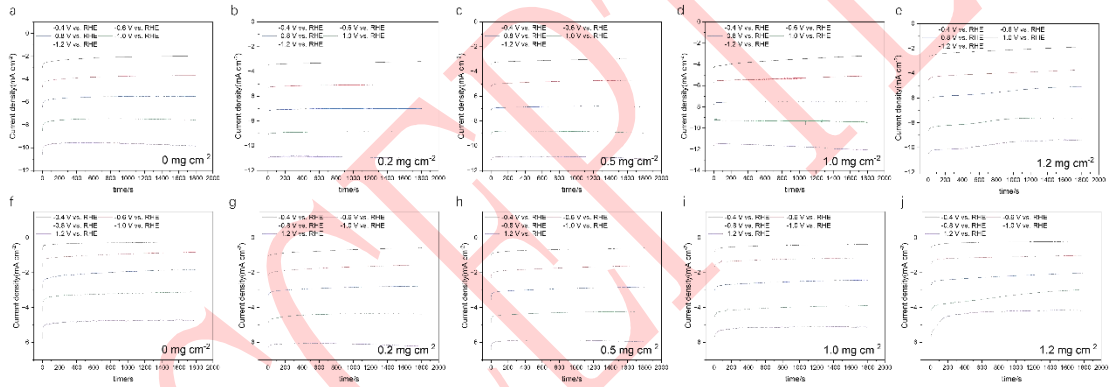


Figure S12. Chronoamperometric current-density–time traces for 30-min electrolysis-side nitrite reduction at different Cu loadings and applied potentials. (a–e) 0.1 M NaOH and (f–j) 0.1 M Na_2SO_4, for nominal Cu loadings of 0, 0.2, 0.5, 1.0, and 1.2 mg cm^{-2}, respectively. Each panel includes -0.4, -0.6, -0.8, -1.0, and -1.2 V vs. RHE. These traces show the recorded current-density evolution during the 30-min potentiostatic electrolysis.

ACCEPTED

Table S1. Average current density (j_{avg}) and total cathodic charge (|Q|) from the 30-min traces in 0.1 M NaOH at -0.8 and -1.2 V vs. RHE (A = 1.77 cm^2; t = 1800 s).

Cu loading	j_{avg}, -0.8 V	|Q|, -0.8 V	j_{avg}, -1.2 V	|Q|, -1.2 V
0	-5.56	17.71	-9.66	30.78
0.2	-7.01	22.35	-10.92	34.79
0.5	−6.85	21.82	−10.91	34.76
1.0	-7.54	24.02	-11.73	37.37
1.2	-5.48	17.46	-9.72	30.97

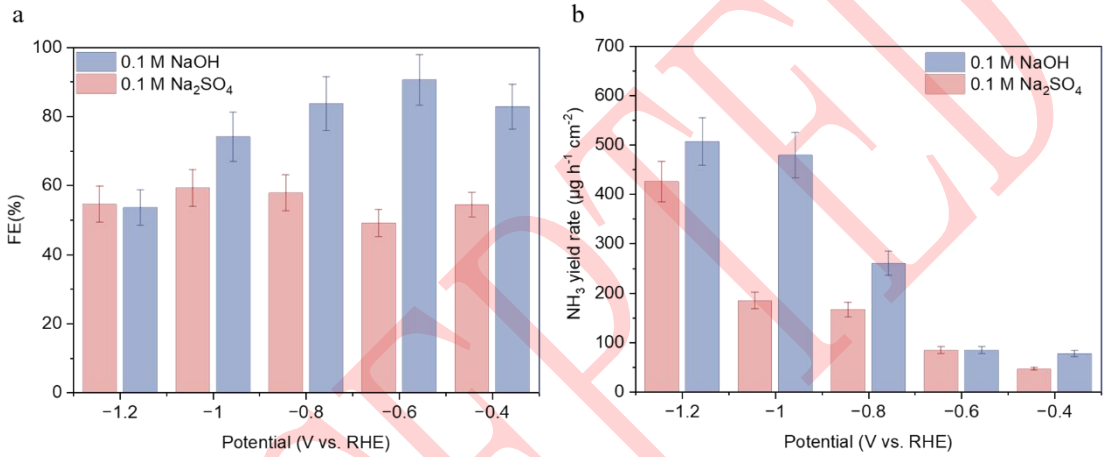


Figure S13. Cu-only control experiments under the same electrolysis-side nitrite-reduction conditions. (a) NH_3 Faradaic efficiency and (b) NH_3 yield rate of Cu foil in 0.1 M NaOH and 0.1 M Na_2SO_4 over -0.4 to -1.2 V vs. RHE.

The values in Table S1 correspond to the representative current–time traces plotted in Figure S12 and are not the group-mean charges used by combining independent runs. For performance statistics, product amount and charge were paired within each replicate before averaging

ACCEPTED

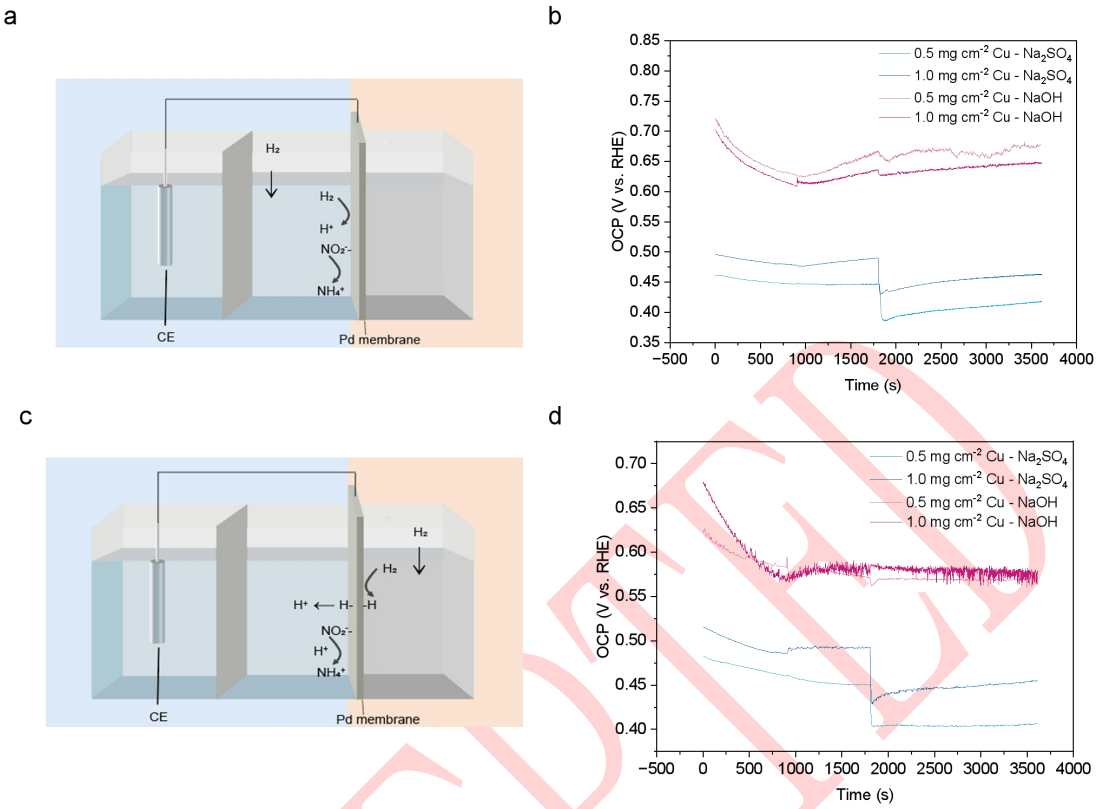


Figure S14. Schematic illustrations of the paired open-circuit H_2-feeding controls and the corresponding OCP traces: (a, b) H_2 is supplied directly to electrolysis chamber II, bypassing transmembrane hydrogen delivery; (c, d) H_2 is supplied to the hydrogenation chamber and reaches the nitrite-containing interface through Pd-membrane permeation. The pair is used to distinguish the effect of transmembrane hydrogen availability from the effect of open-circuit interfacial operation.

ACCEPTED

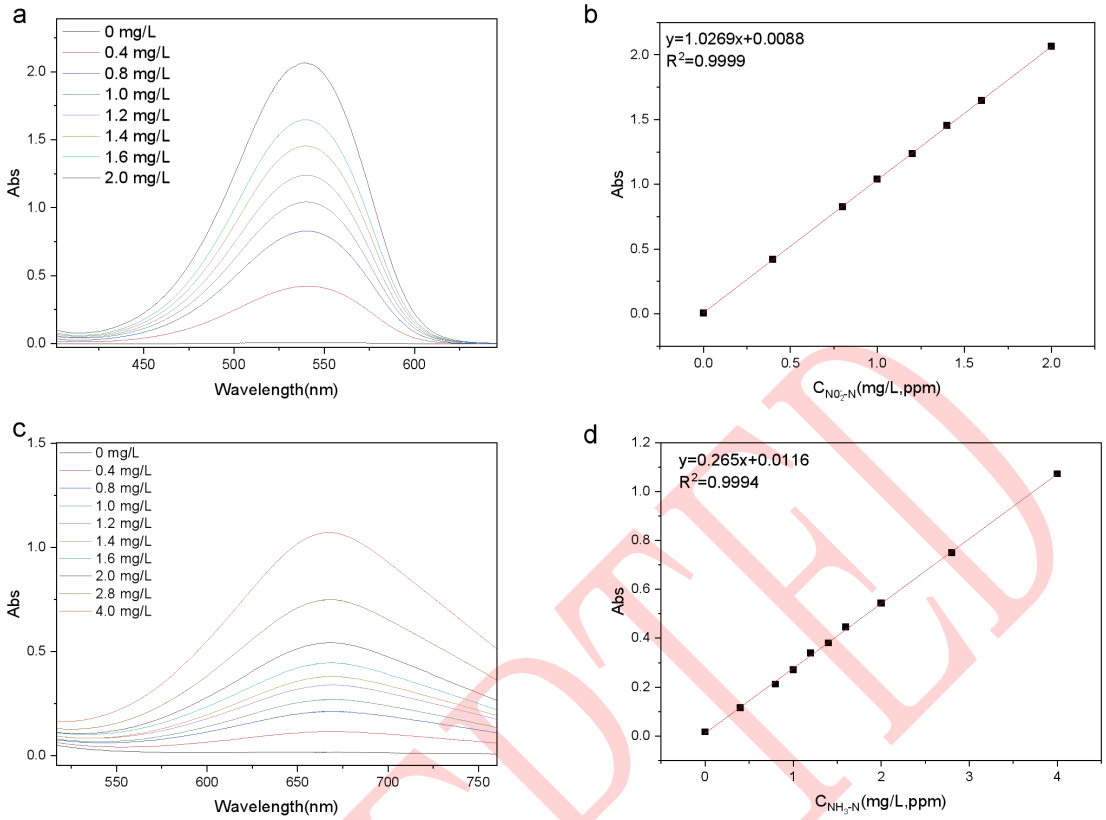


Figure S15. Ultraviolet-visible (UV-Vis) absorption spectra and corresponding calibration curves for the quantification of NO_2^- and NH_3.

ACCEPTED